

Automated calculation of the axial orientation of intravascular ultrasound images by fusion with biplane angiography

Andreas Wahle, Guido P. M. Prause,
Clemens von Birgelen,*
Raimund Erbel,* Milan Sonka

The University of Iowa, Iowa City, IA 52242-1527, USA

*University Hospital Essen, D-45122 Essen, Germany

Poster Layout:

(for information only, not a part of the poster)

| | | | | | | |
|------------------|--------------------------------|-------------------------------|-----------------------------------|------------------------------|---------------------|-----------------------|
| Title | Figure Basics 5 | Figure Cath Bend. 9 | Flowchart Method Outline 13-16 | | 5. Results 21 | Figure VRML 25 |
| Abstract 2 | 3. Previous Work 6 | 4. Absolute Orientation 10 | | | 6. Discussion 26 | |
| 1. Problem 3 | 3.1 Fig. Angio + Catheter 7 | Outline Method 11 | 4.1 Out-of-Center Vecs 17 | 4.2 Reliability Weight 19 | Curves 23 | 7. Conclusions 27 |
| 2. Solution 4 | 3.2 Relative Twist 8 | Angio vs. IVUS 12 | Local Functions 18 | 4.3 Error Minimization 20 | Curves 24 | Further Reading 28 |

ABSTRACT

This poster presents an approach for fusion of the two major cardiovascular imaging modalities, angiography and intravascular ultrasound (IVUS). While the path of the IVUS catheter, which follows the vessel curvature during pullback, is reconstructed from biplane angiograms, cross-sectional information about the vessel is derived from IVUS. However, after mapping of the IVUS frames into their correct 3-D locations along the catheter path, their orientations remain ambiguous. We determine the relative catheter twisting analytically, followed by a statistical method for finding the absolute orientation from the out-of-center position of the IVUS catheter. Our results as obtained from studies with cadaveric pig hearts and from three patients undergoing routine coronary intervention showed a good match of the absolute orientation by the algorithm. In all tested cases, the method determined the visually correct orientations of the IVUS frames. Local distortions were reliably identified and discarded.

1. PROBLEM

- From *biplane angiography*, the 3-D geometry of a vessel can be assessed; however, no information about vessel wall and plaque is provided.
- *Intravascular ultrasound (IVUS)* provides accurate information about vessel wall and the composition of plaque, but current 3-D reconstruction systems do not consider the following effects:
 - Due to vessel *curvature*, the IVUS slices are not parallel, and thus 3-D quantifications based upon conventional straight stacking distorted.
 - Due to vessel *torsion* as defined by differential geometry, the axial orientation of an ideal IVUS catheter within the vessel is no longer constant.

2. SOLUTION

- Combination (*fusion*) of the data obtained from biplane coronary angiography and intravascular ultrasound provides an exact assignment of the cross-sectional data to the vessel segment in both location and orientation:
 1. Both angiograms and all IVUS images are *segmented* to obtain (a) the longitudinal geometry of the vessel, and (b) the cross-sectional information.^[1, 2, 4]
 2. Each IVUS frame can be assigned to a specific *location* from its time-stamp.^[5, 6]
 3. The orientation of an IVUS frame consists of a *relative* portion, defining the relations between adjacent frames,^[3] as well as an *absolute* orientation for the entire frame set.
- This poster focuses on the last item for calculation of the axial orientation in 3-D.

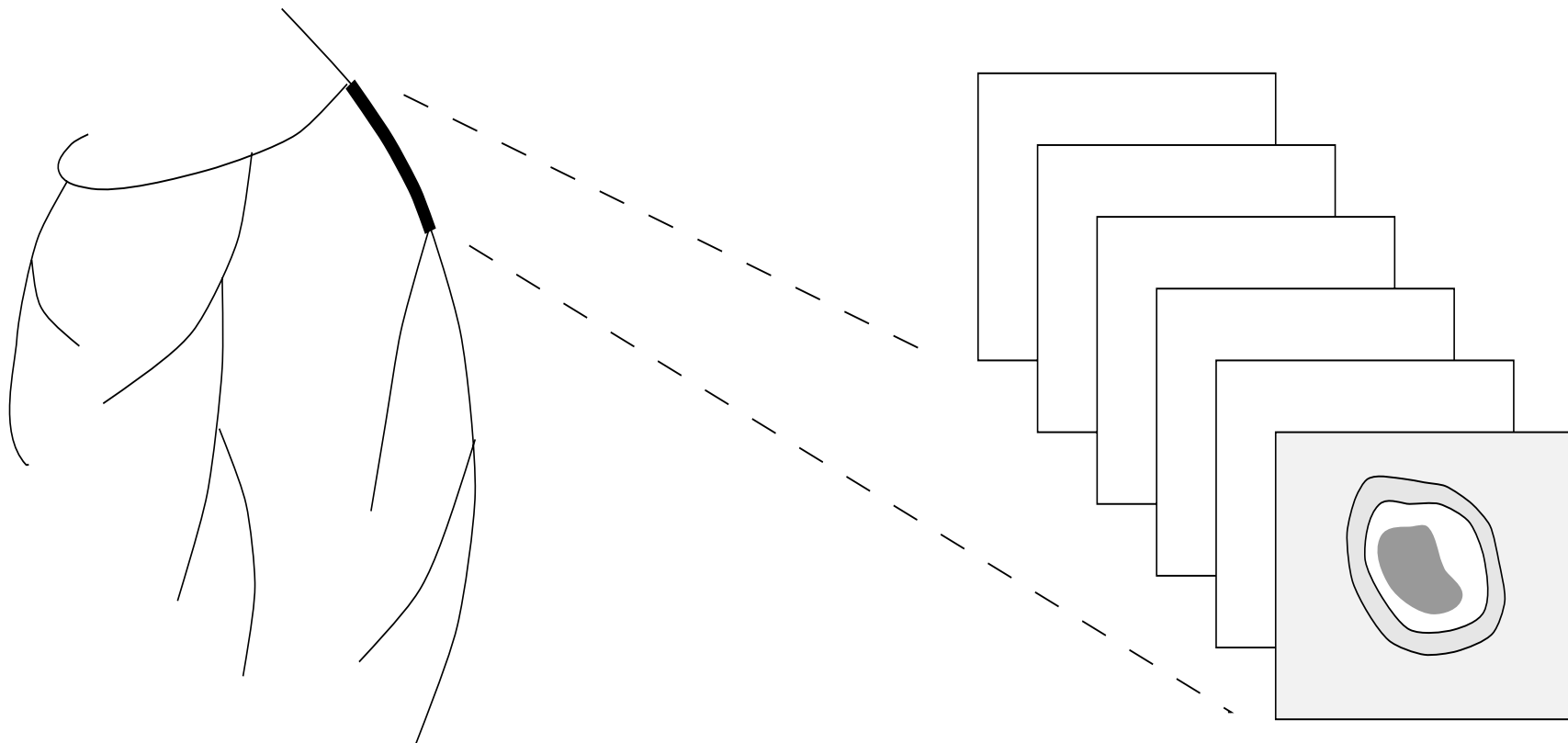


Figure 1: Principle of the fusion approach — the IVUS frames are mapped on their respective location along the 3-D trajectory of the imaging catheter, and their correct spatial orientation is determined.

3. PREVIOUS WORK

3.1 3-D Catheter Trajectory

- Basis for the assignment of the IVUS frames is the 3-D path of the imaging catheter (*trajectory*); after extraction of the 2-D angiographic information, it can be reconstructed using the *epipolar constraint*.^[1]
- The 3-D pullback trajectory is used to assign a specific *3-D location* for each IVUS frame based upon the time-distance function.^[5, 6]
- A *constant pullback speed* is required for this matching (e.g. automated devices), as well as *ECG-gating* in-vivo.

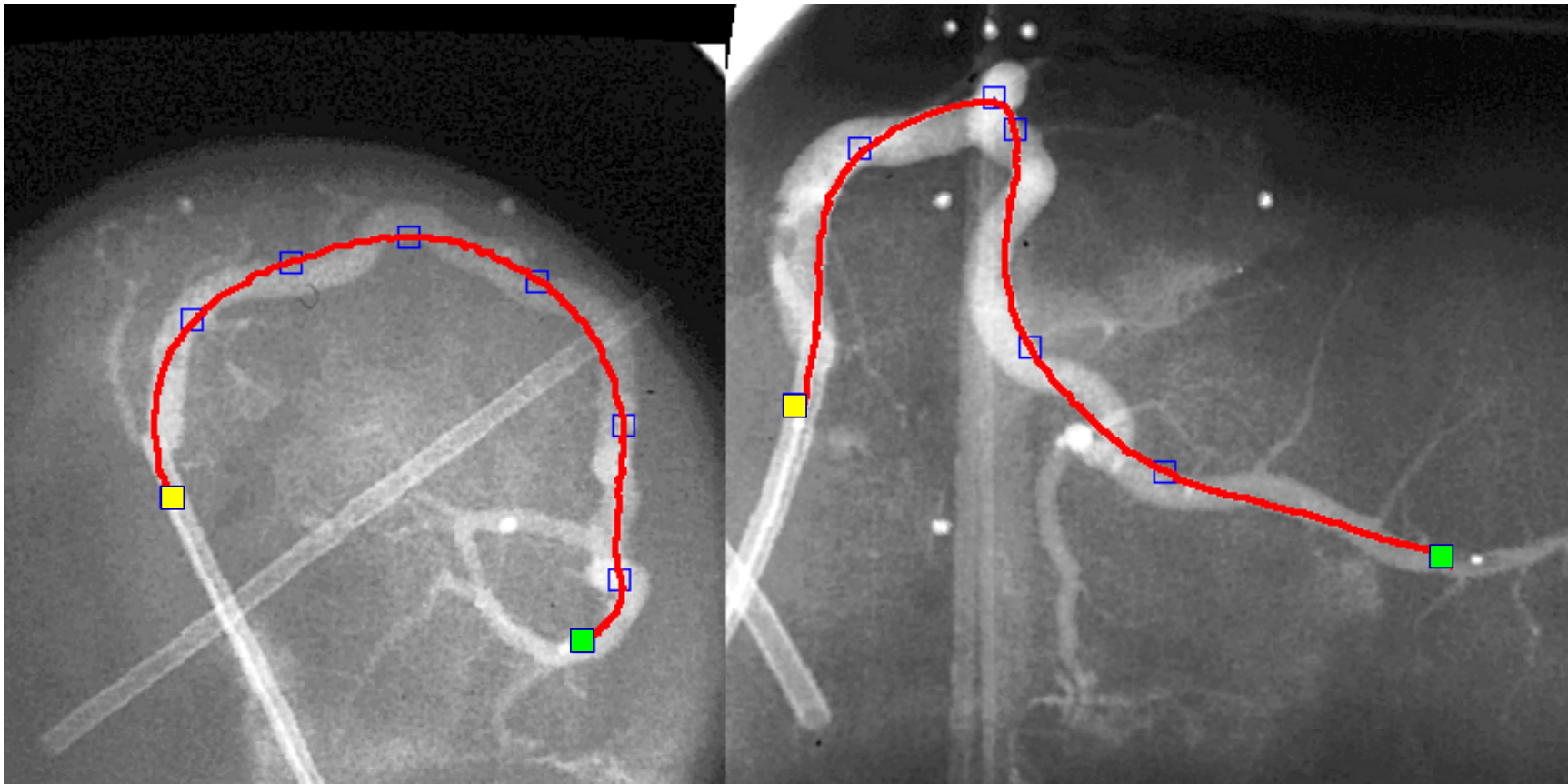


Figure 2: Extraction of the catheter path — transducer marked at the most distal position in both projections (green), along with presumed proximal end of the pullback (yellow), and some guide points outlining the catheter path inbetween.

3.2 Relative IVUS Frame Orientation

The relative orientation changes (*twist*) between adjacent frames are calculated using our *sequential triangulation method*.^[3]

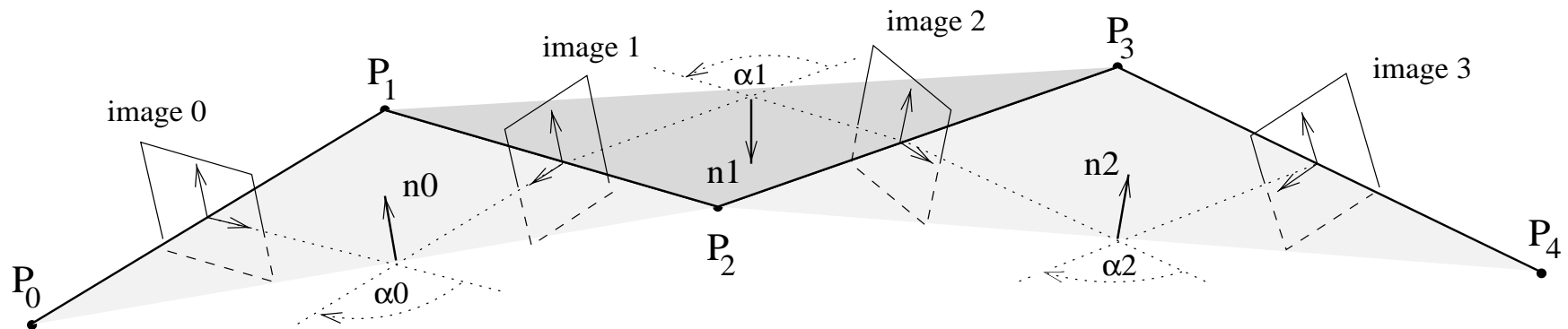


Figure 3: Sequential triangulation — (1) Use the three points of the catheter path next to the frames, (2) calculate circumscribing circle, (3) rotate previous frame around the normal n_i of the circle by the enclosed angle α_i .

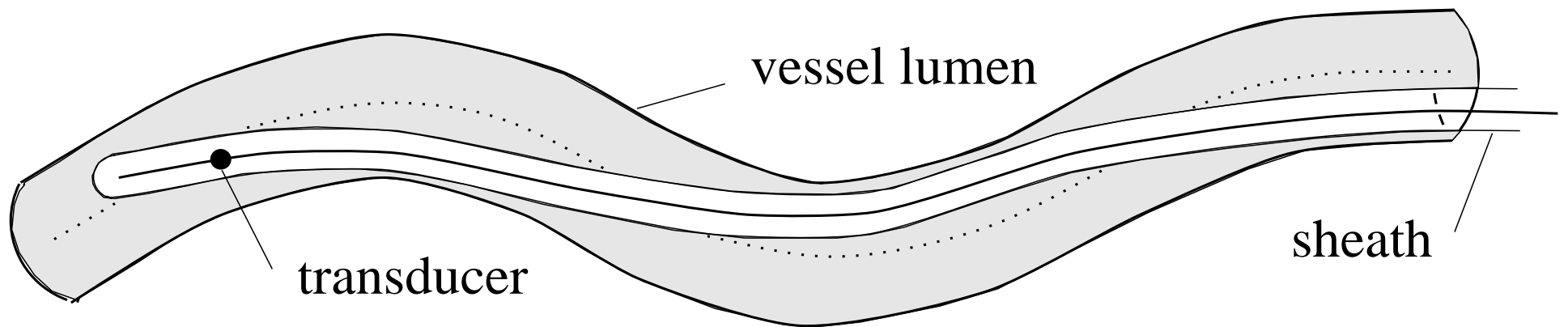


Figure 4: Bending of the imaging catheter within the vessel due to vessel curvature — the catheter is seeking a position of minimum energy and thus provides an artificial landmark for the absolute orientation; the position of the sheath within the vessel remains stable during pullback of the core with the transducer.

4. ABSOLUTE FRAME ORIENTATION

- The sequential triangulation method delivers the *relative* orientation only;
- *leg-sock problem*: the frame set (“sock”) may be rotated arbitrarily around the catheter path (“leg”);
- natural landmarks like branches are often unreliable, artificial landmarks like clips not applicable in-vivo.

- The catheter always seeks a position of *minimum bending energy* within the vessel;
- the *out-of-center position* of the catheter can be identified after segmentation in both angiograms and IVUS images;
- an *error minimization algorithm* based upon statistics in a moving window along the catheter path is used for optimizing the axial orientation in a single correction step.

Outline of our new method:

1. The 3-D catheter path is reconstructed from the angiograms;
2. the *vessel outline*, i.e. the inner lumen contour, is extracted from both angiographic and IVUS data;
3. the relative catheter twist is determined analytically;
4. the IVUS lumen contours are mapped into 3-D space using an *initial orientation*;
5. for each frame location, *out-of-center strength* μ and *difference angles* φ are determined;
6. within a *moving window*, strength and angle values are statistically analyzed;
7. a *reliability weight* is calculated for each window location;
8. finally, a *single correction angle* is derived from all window locations and applied to the frame set.

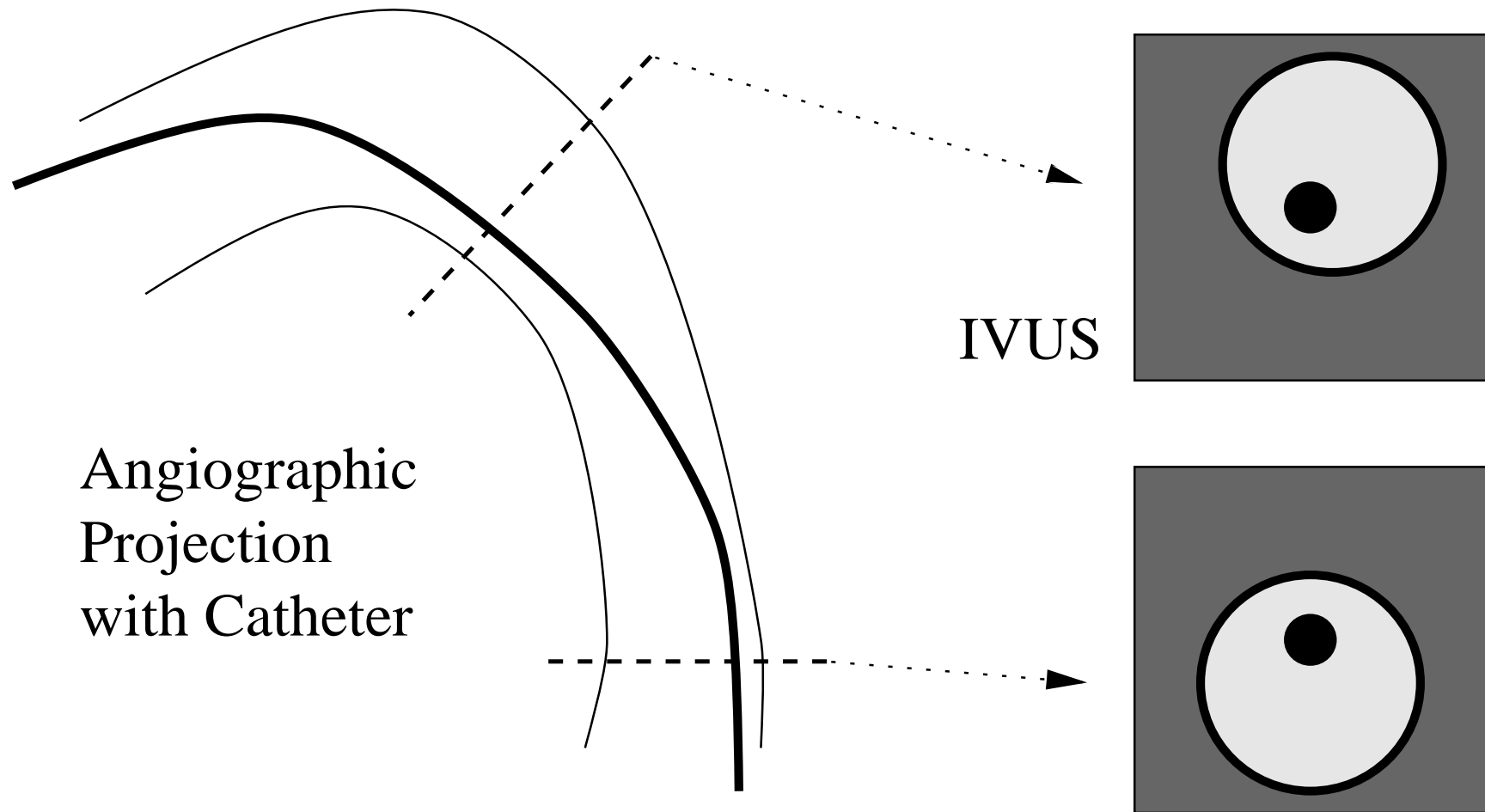
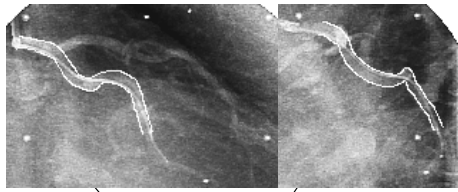


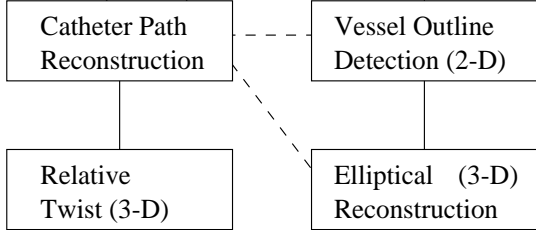
Figure 5: Appearance of out-of-center position of the imaging catheter in angiographic and IVUS images.



Angiograms

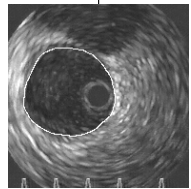
RAO

LAO



Initial Orientation

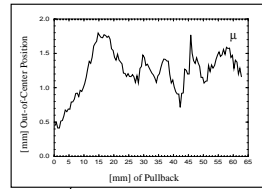
Lumen (2-D) Segmentation



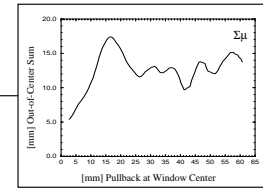
IVUS Data

Out-of-Center Vectors (3-D)

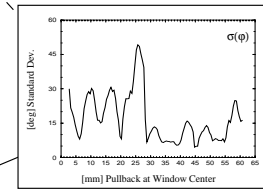
Out-of-Center Strength



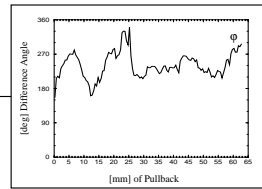
Sum over Moving Window



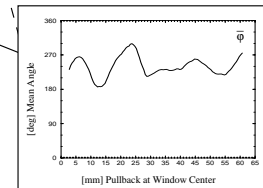
Standard Deviation



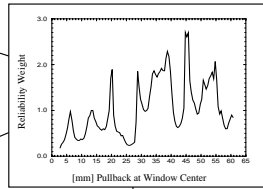
Difference Angle Angio vs. IVUS



Weighted Mean Angle



Reliability Weight



Calculation of Correction Angle

Reconstruction before and after Adjustment

FRONTAL

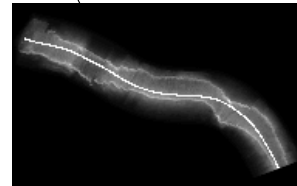
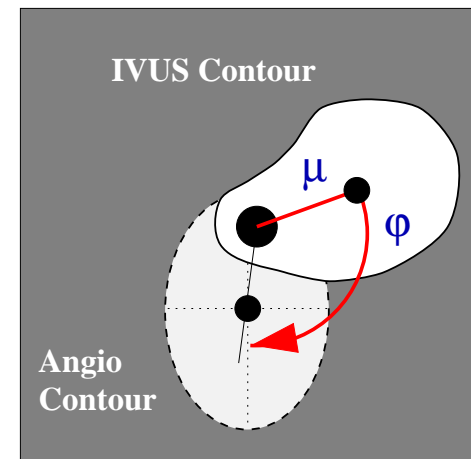


Figure 6: Flow-chart for the absolute orientation assessment.

4.1 Out-of-Center Vectors

- Out-of-center vectors are obtained for each IVUS frame:
 - From angiography
 1. The elliptical cross-sections are reconstructed from the vessel outline;
 2. the intersection of the catheter path with the generated ellipse is determined at the level of the corresponding IVUS frame;
 3. out-of-center vector results from the 3-D vector beginning at this intersection point and ending at the center of the ellipse.

- From IVUS
 1. The centroids are calculated for each mapped IVUS contour;
 2. out-of-center vector results from the 3-D vector beginning at the catheter location and ending at the centroid.
- Two functions are created with the following values for each IVUS frame:
 - The *out-of-center strength* μ is the length of the IVUS out-of-center vector;
 - the *difference angle* φ is the signed angle between the IVUS and the angiographic out-of-center vectors.



4.2 Reliability Weight

- Philosophy:
 - Give higher weight to values with a high out-of-center strength μ ;
 - limit the weight of those with a high tolerance in the angle function φ .
- Realization:
 - Moving window; for each window location k
 1. all difference angles φ_i within k are weighted by their corresponding vector lengths μ_i ;
 2. the *weighted mean* $\bar{\varphi}_k$,
 3. the *weighted standard deviation* $\sigma(\varphi_k)$, and
 4. the *sum of weights* $\Sigma\mu_k$ are derived.

4.3 Error Minimization

After calculation of the reliability function over all windows, the values are combined to a single correction angle:

- The *positive weight* (i.e. locations with increased significance for the estimation of the correction angle) is the sum of weights $\Sigma\mu_k$,
- the *negative weight* (i.e. locations with distorted out-of-center data) results from the local tolerances $\sigma(\varphi_k)$;
- the *correction angle* results from the weighted mean

$$\bar{\varphi}_{\text{corr}} = \sum_k \left(\bar{\varphi}_k \frac{\Sigma\mu_k}{\sigma(\varphi_k)} \right) / \sum_k \left(\frac{\Sigma\mu_k}{\sigma(\varphi_k)} \right)$$

and is applied to all IVUS frames.

5. RESULTS

- The fusion approach was validated in a series of in-vitro studies using computer models, phantoms, and cadaveric pig hearts;^[3, 5]
- manual pullback introduces unacceptable localization errors due to inhomogeneous speed, thus automated pullback was applied in-vivo;
- biplane angiographic images were acquired digitally;
- our approach was successfully applied to three patients with stable coronary artery disease, undergoing coronary revascularization and stent placement in native coronary arteries, and which were imaged as part of their clinical procedure;
- visualization was performed by both generation of a 3-D voxel cube mapped from IVUS pixel data, and as VRML model.^[6]

Example:

The following figures show the analysis of a stenosed segment in a left coronary artery, 40 mm in length.

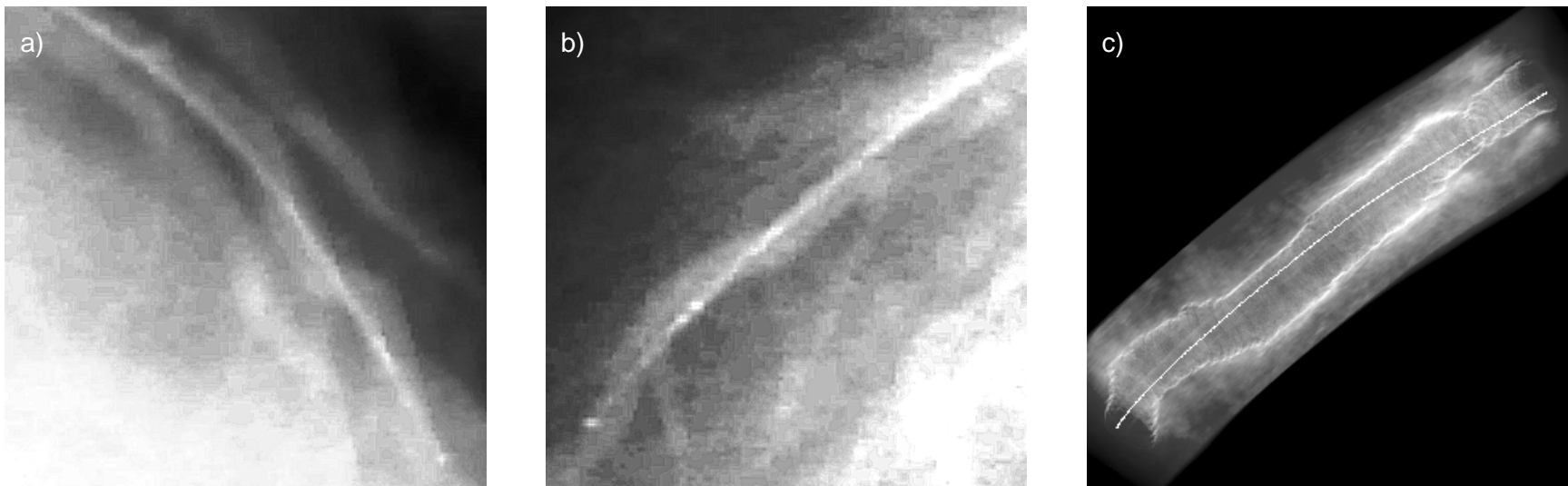


Figure 7: Detail in a) 30° RAO and b) 60° LAO projections of a left anterior descending artery; c) transmission image through IVUS cube in lateral view.

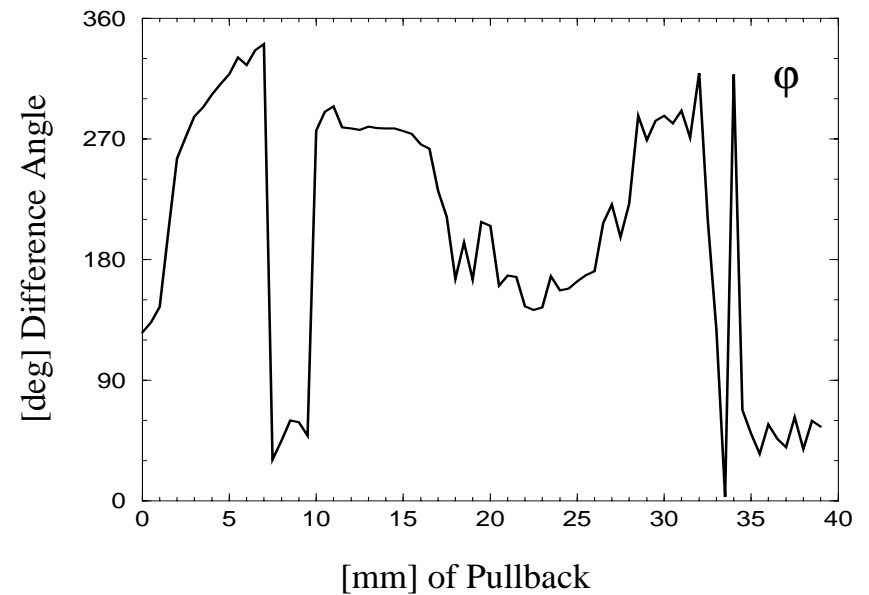
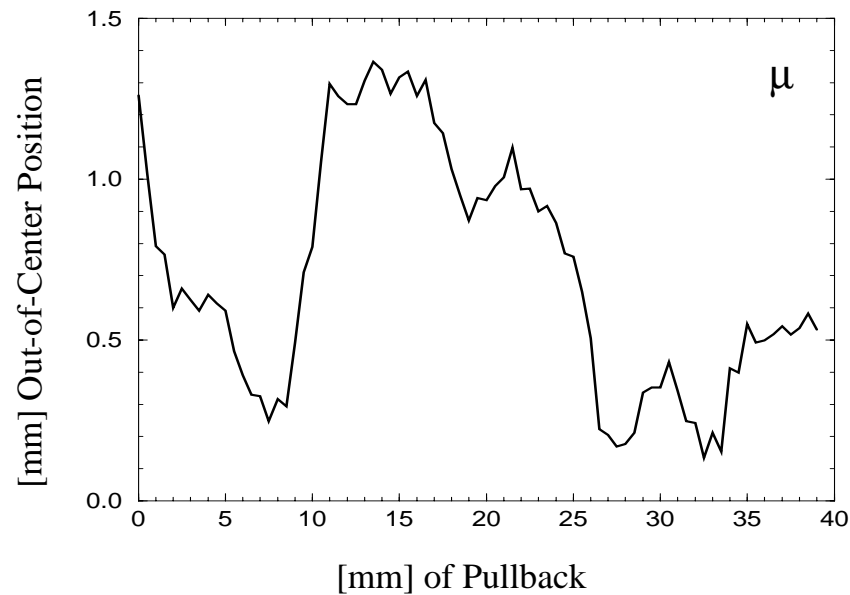


Figure 8: Functions for length μ of the out-of-center vector and local correction angle φ of the human artery shown in Figure 7; note the high variances in the angle function when the out-of-center position falls below angiographic resolution (<0.5 mm).

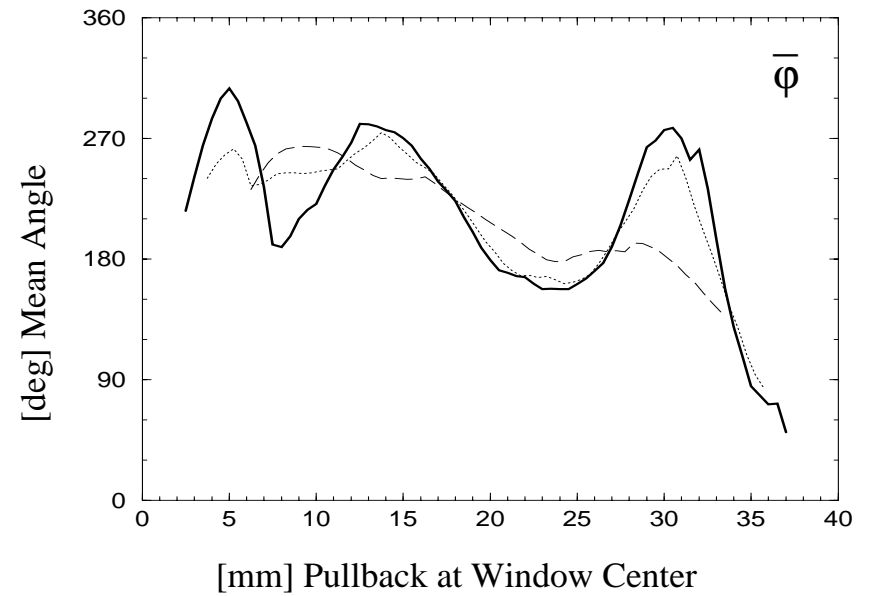
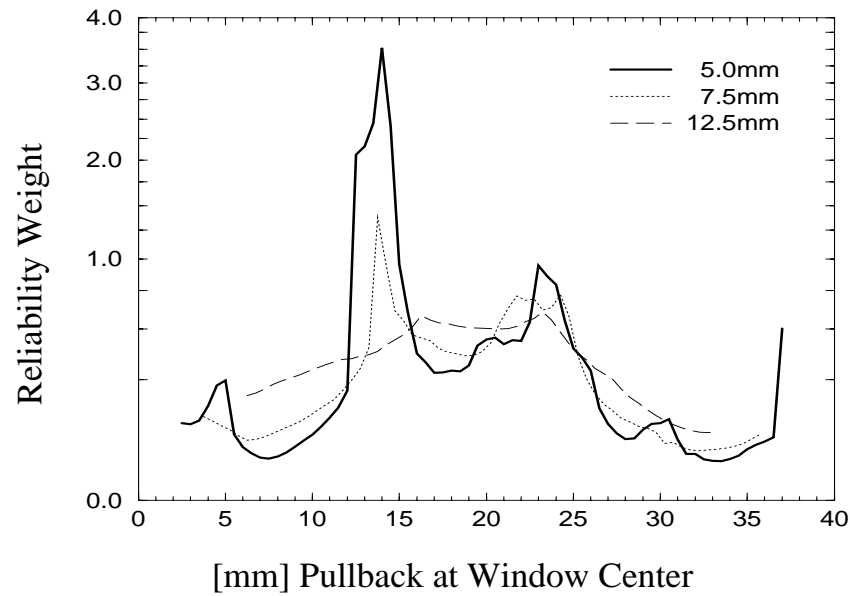


Figure 9: Final functions for reliability weight $\Sigma\mu_k/\sigma(\varphi_k)$, with non-linear scale to allow a better visual comparison of the curves, and weighted mean difference angle $\bar{\varphi}_k$, for each location of the moving window in three different sizes.

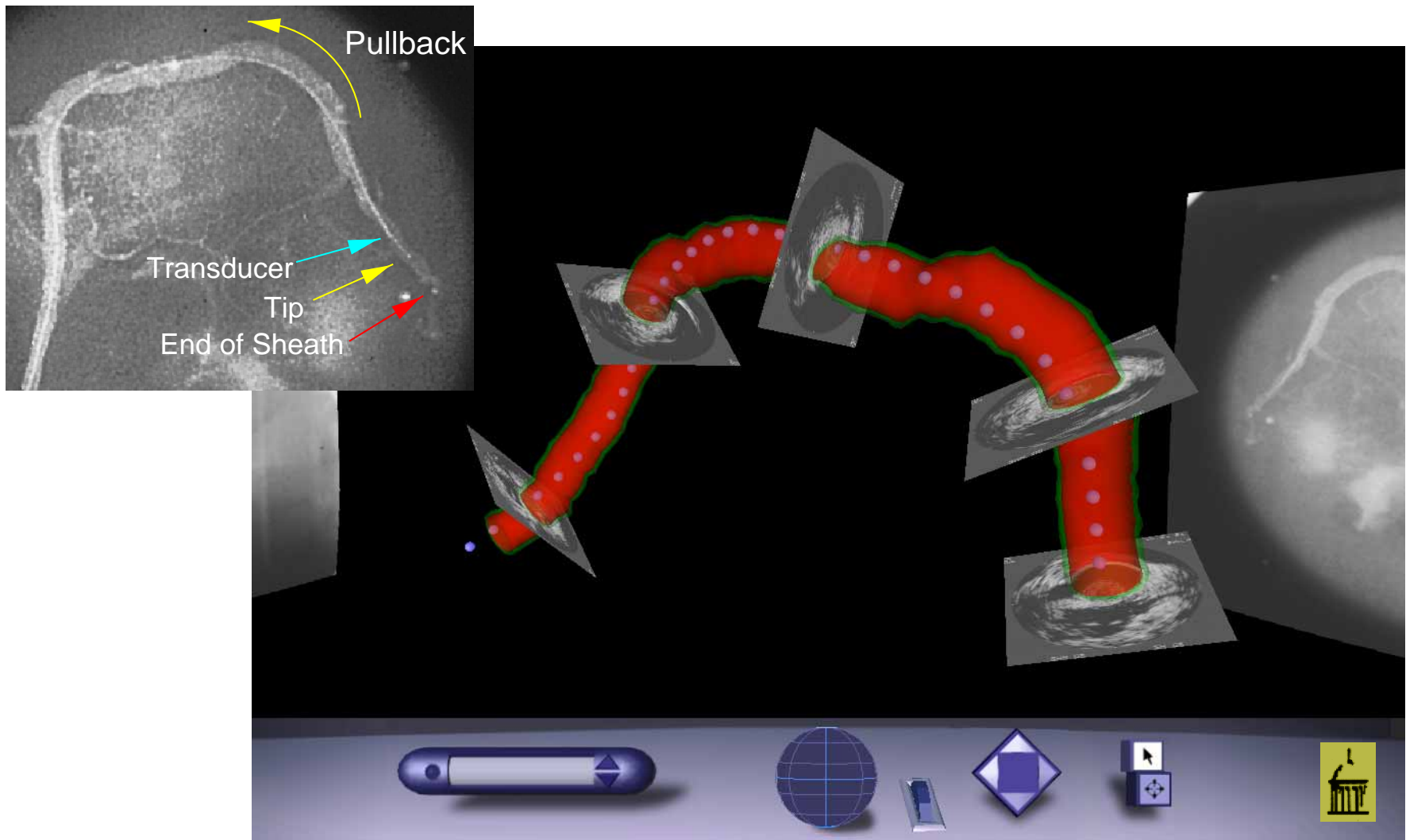


Figure 10: Angiogram and interactive VRML visualization of the right coronary artery of a cadaveric pig heart.

6. DISCUSSION

- The presented method has a high potential to overcome a major problem in the determination of the absolute orientations of the IVUS frames;
- using the catheter itself as an artificial landmark does avoid the need for detecting frequently unreliable natural landmarks or the application of markers directly on the vessel;
- IVUS imaging catheters in sheathed design along with automated pullback are mandatory;
- strong angiographic foreshortening should be avoided to allow optimal performance of our algorithm for the determination of the absolute orientation;
- the developed system has shown to be robust against distorting influences, and misinterpretations occur only in severe cases.

7. CONCLUSIONS

- A comprehensive approach to fusion of intravascular ultrasound and biplane angiography has been developed, validated, and applied in-vitro as well as in-vivo.
- Using IVUS catheters in sheathed design, the absolute orientation of the IVUS frame set is directly determined from the out-of-center position of the imaging catheter.
- By the introduction of a reliability weight along with our moving window technique, possible errors are successfully detected and discarded.
- The presented fusion approach delivers high-quality 3-D IVUS reconstructions, operates on a highly automated level, and thus substantially improves the clinical applicability of cath-lab imaging.

Further Reading

- [1] A. Wahle, E. Wellnhofer, I. Mugaragu, H. U. Sauer, H. Oswald, and E. Fleck, “Assessment of diffuse coronary artery disease by quantitative analysis of coronary morphology based upon 3-D reconstruction from biplane angiograms,” *IEEE Transactions on Medical Imaging* **14**, pp. 230–241, June 1995.
- [2] M. Sonka, X. Zhang, M. Siebes, M. S. Bissing, S. C. DeJong, S. M. Collins, and C. R. McKay, “Segmentation of intravascular ultrasound images: A knowledge-based approach,” *IEEE Transactions on Medical Imaging* **14**, pp. 719–732, Dec. 1995.
- [3] G. P. M. Prause, S. C. DeJong, C. R. McKay, and M. Sonka, “Towards a geometrically correct 3-D reconstruction of tortuous coronary arteries based on biplane angiography and intravascular ultrasound,” *International Journal of Cardiac Imaging* **13**, pp. 451–462, Dec. 1997.
- [4] C. von Birgelen, E. A. de Vrey, G. S. Mintz, A. Nicosia, N. Bruining, W. Li, C. J. Slager, J. R. T. C. Roelandt, P. W. Serruys, and P. J. de Feyter, “ECG-gated three-dimensional intravascular ultrasound: Feasibility and reproducibility of the automated analysis of coronary lumen and atherosclerotic plaque dimensions in humans,” *Circulation* **96**, pp. 2944–2952, Nov. 1997.
- [5] A. Wahle, G. P. M. Prause, S. C. DeJong, and M. Sonka, “3-D fusion of biplane angiography and intravascular ultrasound for accurate visualization and volumetry,” in *Medical Image Computing and Computer-Assisted Intervention (MICCAI '98)*, W. M. Wells *et al.*, eds., pp. 146–155, Springer, (Berlin/New York), 1998.
- [6] S. C. Mitchell, A. Wahle, C. von Birgelen, R. Erbel, and M. Sonka, “Real-time visualization of coronary interventions using VRML,” in *Proc. Medical Imaging 1999: Physiology and Function from Multidimensional Images, San Diego CA*, No. 3660-31, SPIE, (Bellingham WA), Feb. 1999.